Second-harmonic response and temperature differential resistivity of noncollinear spin valves

Julie Dubois[1,2] and Jean-Philippe Ansermet[1]
[1]*Institut de Physique des Nanostructures, Ecole Polytechnique Fédérale de Lausanne (EPFL), Station 3, CH-1015 Lausanne, Switzerland*
[2]*Ecole des Mines, 60 Boulevard Saint Michel, 75006 Paris, France*
(Received 4 July 2008; revised manuscript received 27 September 2008; published 21 November 2008)

By means of a diffusive description of spin-dependent thermal and electrical transport using Pauli-spin matrices, we analyze the spin-dependent transport mechanisms that determine the voltage response of a metallic spin valve to an ac temperature oscillation under steady current and the second-harmonic voltage response to spin-torque induced oscillations of the magnetization of the layers. We show the extent to which both measurements are sensitive to the relaxation of the transverse spin moment. The simulations of these signals suggest an experimental protocol to characterize the decay of the spin-accumulation precession due to *s-d* interaction in ferromagnets.

DOI: 10.1103/PhysRevB.78.184430 PACS number(s): 72.25.−b, 72.15.Gd, 73.23.−b, 75.47.De

I. INTRODUCTION

The notion that a spin-polarized current can act on the magnetization was announced in two seminal papers by Berger[1] and Slonczewski.[2] With time, it became clear that this torque arises when the conduction electrons enter a layer where the magnetization is not aligned with their spin polarization and that this torque is linked to the absorption or relaxation of the transverse component of the spin polarization.[3] The spin polarization is an out-of-equilibrium property that arises when a current is driven through a magnetic nanostructure: a so-called spin accumulation builds up in spin valves as a consequence of the differences in the conductivities of each spin channel in successive layers.[4] When the magnetizations of the two layers of a spin valve are not collinear, the spin accumulation of the incoming electrons is at an angle with respect to the magnetizations.[5] For Slonczewski,[6] the length over which this transverse component decays is of the order of 1 a.u., owing to the distribution of the effective exchange field on the Fermi surface. However, Shpiro *et al.*,[7] who described this decay in a self-consistent model in a diffusive regime, estimated this decay length to be in the range of a few nanometers.[8]

In this paper, we use a thermodynamic approach to describe heat, spin, and charge currents in magnetic nanostructures in noncollinear configurations. As reported by other groups, we describe the spin and charge currents as tensorial quantities using Pauli matrices.[9] We follow the notation of Zhang *et al.*[10] A thermodynamic description of spin-dependent transport was initiated by Johnson and Silsbee,[11,12] providing much information on spin accumulation in a van der Pauw structure.[13] This formalism allowed Wegrowe *et al.*[14] to express the details of *s* and *d* electron-spin-relaxation processes. The Onsager matrix which links generalized currents and generalized forces (gradients of their associated potentials)[15] brings forth automatically the possibility of spin mixing.[16] By definition, spin mixing is a nonresistive process in the sense that the electron momentum before and after a collision is conserved. In bulk materials, spin mixing is expected due to the collision of electrons with magnons.[17,18] In spin valves, when a conduction electron enters a magnetic layer from a nonmagnetic metal, its spin experiences a sudden turn on of a magnetic field. The spin dynamics are the extreme opposite to the adiabatic passage as found, for example, when an electron crosses a domain wall.[19] Following Shpiro *et al.*,[7] we express this with a Bloch equation for the transverse spin accumulation [see Eq. (9) below]. The precession here plays the role of spin mixing. Brataas *et al.*[5] instead used quantum mechanics to calculate the spin-mixing conductivities at interfaces, thus setting the boundary conditions for diffusive transport in each layer. These calculations were later extended in order to include thermal currents.[20] Zhang and Levy[21] studied the time-dependent diffusion equation and compared that prediction with the stationary diffusive model in the stationary limit, as well as the predictions based on the Boltzmann transport equation.[22,23] Our thermodynamic description of spin-dependent transport is sufficient to analyze two experimental methods. One is the measurement of the derivative with respect to the temperature of the resistance of the nanostructure under test. The other is the measurement of the second-harmonic response of a spin valve subjected to an alternating current.

We call the first measurement the magnetothermogalvanic voltage (MTGV). It consists in enforcing a small oscillation of the temperature of the sample and measuring its resistance as a function of magnetic field.[24] A small modulation of the temperature T_0 is produced by illuminating the sample with a laser beam of about 10 W cm^{-2}, chopped at a frequency of 14–22 Hz. A dc is driven through the structure and the ac voltage is detected at the chopping frequency. The MTGV is highly sensitive to phenomena that occur during reversible switching of magnetic layers. Gravier *et al.*[25] established the link between MTGV and spin mixing through a three-current model: a heat current and spin-up and spin-down electrical currents. In this paper we compute the MTGV signal from our noncollinear model and confirm its link to spin mixing in the sense that we find that the signal depends on the temperature dependence of the decay length of the transverse component of spin accumulation.

The second experiment analyzed in the framework of our model is an electrical detection of the small perturbation of the magnetization of the free layer of a spin valve, induced by the spin torque due to spin-polarized currents. Kovalev *et al.*,[26] for example, calculated the deviation of magnetization

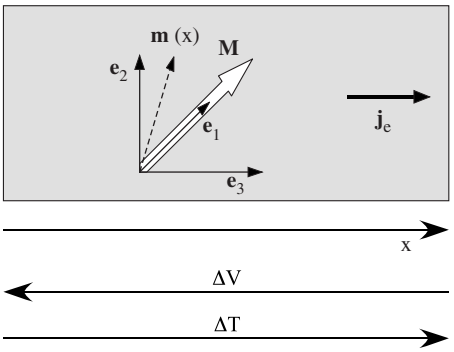

FIG. 1. Schematics of one magnetic layer: **M** is the magnetization, with $(\mathbf{e}_1,\mathbf{e}_2,\mathbf{e}_3)$ as the local orthogonal basis of magnetization defined by **M** ($\mathbf{e}_1$ is parallel to **M** shown here out of the plane of the paper). ΔT and ΔV are the temperature and potential drops, j_e the charge current, and $m(x)$ the spin-accumulation vector.

orientations in spin valves due to spin torque. We follow the concept to evaluate the double-frequency signal induced in a spin-valve structure under a nonresonant current. We find that this double-frequency detection can lead to a new experimental measurement of the characteristic length of the relaxation of the transverse component of the spin-accumulation vector.

The paper is structured as follows. In Sec. II we start from Onsager relations linking generalized currents to their associated forces. We express the coupling of the conduction-electron spins to the magnetization in continuity equations in order to develop the diffusive model. Section III presents the results of simulations when we apply the model to a spin valve or to two magnetic electrodes separated by a thin metal layer. Simulations of MTGV and double-frequency signals are described and analyzed. Finally, in Sec. IV, we discuss the macrospin approximation of our model and the influence of an inhomogeneous local magnetization on our results.

II. THERMODYNAMIC DESCRIPTION OF SPIN, CHARGE, AND HEAT CURRENTS

A. Constitutive equation of currents and potential

We consider a one-dimensional (1D) model of a magnetic multilayer with current flow perpendicular to the interfaces (the variable x will be used as the spatial coordinates). In Fig. 1 we have represented one magnetic layer to which we will apply the following description. We will then apply this model to a ferromagnetic-metal-nonmagnetic-metal-ferromagnetic-metal (F/N/F) spin valve (Fig. 2) for computation.

We know that our samples have rather disordered interfaces because of the method of their production. So we consider sufficient a semiclassical approach based on the developments made by Zhang *et al.*[10] and Shpiro *et al.*[7] The diffusive nature of our samples implies also that thermalization is obtained for the spin-up and spin-down channels, so that we do not have to introduce a bias temperature as exists in a ballistic treatment of a spin-valve system.[19] The analysis of Levy and Zhang,[22,23] based on the Boltzmann equation in

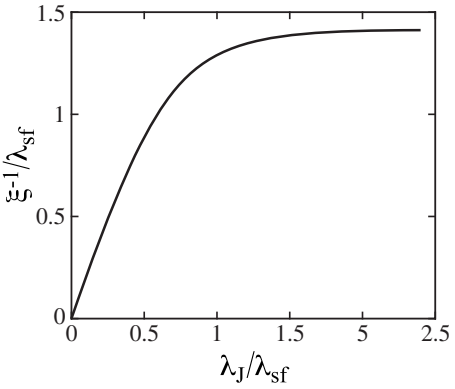

FIG. 2. Ratio ξ^{-1}/λ_{sf} as a function of λ_J/λ_{sf}: slope of $\sqrt{2}$ and asymptote of $\sqrt{2}$ for small and large values of λ_J/λ_{sf}, respectively.

Pauli space or the time-dependent diffusive description,[21] shows the extent of corrections to the stationary diffusive model[7,10] in the case of sharp interfaces.

We also assume that the temperature gradient is small enough so the conduction tensors are uniform in space to first order, equal to their value at T_0, the average temperature of the structure. The Onsager reciprocal relations including the thermal current[27] are written in the Pauli space as follows,[28] expanding Zhang *et al.*[10] and Shpiro *et al.*:[7]

$$\hat{j}(x) = \hat{C}\left(E(x)\hat{\mathbf{I}} + \frac{1}{e}\frac{\partial\hat{\mu}}{\partial x}\right) - \hat{K}\frac{\partial T}{\partial x},$$

$$j_q(x) = T_0\hat{K}:\left(E(x)\hat{\mathbf{I}} + \frac{1}{e}\frac{\partial\hat{\mu}}{\partial x}\right) - \mathrm{Tr}(\hat{L})\frac{\partial T}{\partial x}, \tag{1}$$

where E is the electric field, T the temperature, j_q the heat current, $\hat{\mathbf{I}}$ the identity matrix, and the symbol ":" refers to the contracted product of two tensors. The current $\hat{j}$, the chemical potential $\hat{\mu}$, and the Onsager coefficients $\hat{C}$, $\hat{K}$, and $\hat{L}$ are 2×2 tensors, which can be decomposed on the Pauli-spin matrix $\boldsymbol{\sigma}$ and the identity matrix $\hat{\mathbf{I}}$,

$$\hat{C} = c_0\hat{\mathbf{I}} + c\mathbf{M}\cdot\boldsymbol{\sigma}, \tag{2}$$

$$\hat{K} = k_0\hat{\mathbf{I}} + k\mathbf{M}\cdot\boldsymbol{\sigma}, \tag{3}$$

$$\hat{L} = l_0\hat{\mathbf{I}} + l\mathbf{M}\cdot\boldsymbol{\sigma}, \tag{4}$$

$$\hat{\mu} = \mu_0\hat{\mathbf{I}} + \mathbf{m}\cdot\boldsymbol{\sigma}, \tag{5}$$

$$j_e = \mathrm{Re}[\mathrm{Tr}(\hat{j})],$$

$$\mathbf{j_m} = \mathrm{Re}[\mathrm{Tr}(\hat{j}\boldsymbol{\sigma})], \tag{6}$$

where **M** is the unit vector representing the direction of local magnetization of one layer and **m** has the dimensions of a chemical potential. The generalized charge and spin accumulation $\hat{n}$ is proportional to the chemical potential with $eN(\varepsilon_F)$ as the coefficient of proportionality, where $N(\varepsilon_F)$ is the density of states at the Fermi level,[4]

$$\hat{n} = \int e\hat{N}(E)\hat{f}(E)dE = e\hat{N}(\varepsilon_F)\hat{\mu}.$$

For convenience we note the generalized diagonal field,

$$\mathcal{E} = E(x) + \frac{1}{e}\mathrm{Tr}\left(\frac{\partial\hat{\mu}}{\partial x}\right). \tag{7}$$

We express now the equations of continuity for the currents in the stationary regime. The spin accumulation precesses around the local magnetization **M** due to the *s-d* interaction and relaxes due to the spin-flip scattering of conduction electrons with a characteristic time t_{sf}.[7,10] In Eq. (9) below, we deduce the motion of **m** from the equation of motion of spin accumulation $\hat{n}$, with $\tau_{sf}=t_{sf}/eN(\varepsilon_F)$ and $g=JeN(\varepsilon_F)/\hbar$ are the rescaled parameters of spin flip and spin precession and J the exchange interaction between conduction electrons and the local magnetization through *s-d* interactions.[10] Dissipation arises from the Joule effect, which is written in Pauli space as the trace of the product of the gradient of potentials (chemical and electrical) and the current $\hat{j}$. Thus we obtain the three dispersion equations,

$$\frac{dj_e}{dx} = 0, \tag{8}$$

$$\frac{d\mathbf{j_m}}{dx} = \frac{\mathbf{m}}{\tau_{sf}} + g\mathbf{M}\wedge\mathbf{m}, \tag{9}$$

$$\frac{dj_q}{dx} = \mathrm{Tr}\left[\left(E(x)\hat{\mathbf{I}} + \frac{1}{e}\frac{d\hat{\mu}}{dx}\right)\hat{j}\right]. \tag{10}$$

1. Nonmagnetic layers

In nonmagnetic layers, transport matrices (2)–(4) are diagonal. We introduce the following notations:

$$\hat{C} = c_N\hat{\mathbf{I}}, \tag{11}$$

$$\hat{K} = k_N\hat{\mathbf{I}}, \tag{12}$$

$$\hat{L} = l_N\hat{\mathbf{I}}. \tag{13}$$

We develop the transport equation [Eq. (1)] using definitions (11)–(13) to obtain

$$j_e = 2\left[c_N\mathcal{E} - k_N\frac{dT}{dx}\right],$$

$$\mathbf{j_m} = 2\left[c_N\frac{1}{e}\frac{d\mathbf{m}}{dx}\right],$$

$$j_q = 2\left[Tk_N\mathcal{E} - l_N\frac{dT}{dx}\right]. \tag{14}$$

By substituting Eq. (14) into the continuity [Eqs. (8)–(10)] with $\mathbf{M}=0$, we obtain the diffusion equation for the chemical-potential vector and a differential equation for the electrical field, including a term for Joule heating,

$$\frac{c_N}{e}\frac{d^2\mathbf{m}}{dx^2} = \frac{\mathbf{m}}{2\tau_N}, \tag{15}$$

$$2\left[T_0k_N - \frac{l_Nc_N}{k_N}\right]\frac{d\mathcal{E}}{dx} = \mathcal{E}j_e + \frac{c_N}{e^2}\left\|\frac{d\mathbf{m}}{dx}\right\|^2. \tag{16}$$

Defining the spin-diffusion length $q^{-1}=\sqrt{2\tau_Nc_Ne^{-1}}$, the general solution of Eq. (15) is

$$\mathbf{m} = \mathbf{m}_{(+)}\exp(qx) + \mathbf{m}_{(-)}\exp(-qx). \tag{17}$$

In nonmagnetic metals such as copper the spin-diffusion length can be of the order of a few hundreds of nanometers at room temperature.[29,30] But in electrodeposited Co/Cu/Co spin valves, the process introduces Co impurities that reduce the spin-diffusion length in copper to 40 nm.[31,32] As for the characteristic length $(T_0k_N-l_Nc_Nk_N^{-1})j_e^{-1}$, it is more than a hundred of microns for current densities of the order of 10^6 A/cm^2. Thus we can overlook the right-hand term in Eq. (16) and consider $\mathcal{E}$ constant in a nonferromagnetic layer.

2. Magnetic layers

We will consider that the magnetization **M** of a magnetic layer is homogeneous in the following development. Substituting expressions (2)–(6) into the transport equation [Eq. (1)], we can decompose $\hat{j}$ into currents of charge, spin, and heat,

$$j_e = 2\left[c_0\mathcal{E} - k_0\frac{dT}{dx} + \frac{c}{e}\mathbf{M}\cdot\frac{d\mathbf{m}}{dx}\right],$$

$$\mathbf{j_m} = 2\left[\left(c\mathcal{E} - k\frac{dT}{dx}\right)\mathbf{M} + \frac{c_0}{e}\frac{d\mathbf{m}}{dx}\right],$$

$$j_q = 2\left[T_0k_0\mathcal{E} - l_0\frac{dT}{dx} + \frac{T_0k}{e}\mathbf{M}\cdot\frac{d\mathbf{m}}{dx}\right]. \tag{18}$$

We substitute Eq. (18) into the continuity equations [Eqs. (8)–(10)] and split **m** into longitudinal (parallel to **M**) and transverse (perpendicular to **M**) components. Intermediary results are given in the Appendix [Eqs. (A2)–(A5)], where we introduce for convenience the parameters u and v,

$$u = k_0c - c_0k,$$

$$v = k_0c_0 - ck. \tag{19}$$

Thus, keeping only linear terms, we find the differential equations for the diffusion of **m**,

$$P_0\mathcal{F}(m_\parallel) + P_1m_\parallel + P_2\frac{dm_\parallel}{dx} + P_3\frac{d^2m_\parallel}{dx^2} = 0, \tag{20}$$

$$\frac{c_0}{e}\frac{d^2\mathbf{m}_\perp}{dx^2} = \frac{\mathbf{m}_\perp}{2\tau_{sf}} + \frac{g}{2}\mathbf{M}\wedge\mathbf{m}_\perp, \tag{21}$$

where $\mathcal{F}(m_\parallel)=\int_0^x m_\parallel dx+cte$ is a primitive of the longitudinal component and the following coefficients are defined:

$$P_0 = -\frac{k_0}{4\tau_{sf}u} j_e,$$

$$P_1 = \frac{(T_0 k_0^2 - l_0 c_0)}{2u\tau_{sf}},$$

$$P_2 = \left(\frac{v}{2eu} - \frac{k}{2ek_0}\right) j_e,$$

$$P_3 = \frac{1}{e}\left[\left(T_0 k - \frac{l_0 c}{k_0}\right) - \left(T_0 k_0 - \frac{l_0 c_0}{k_0}\right)\frac{v}{u}\right]. \quad (22)$$

It is remarkable that in Eq. (21), the transverse momentum is not affected by the presence of a temperature or potential gradient. For convenience we write $\mathbf{m}_\perp$ as a complex vector,

$$\mathbf{m}_\perp = \mathrm{Re}(m_\perp)\mathbf{e}_2 + \mathrm{Im}(m_\perp)\mathbf{e}_3,$$

and the solution of Eq. (21) in the complex space $\mathbb{C}$ is given by

$$m_\perp = m_{(+)} \exp[(\xi + i\varphi)x] + m_{(-)} \exp[-(\xi + i\varphi)x], \quad (23)$$

where ξ and φ are the real and imaginary parts of the root of Eq. (21),

$$\xi + i\varphi = \left(\frac{e}{2c_0\tau_{sf}} + i\frac{eg}{2c_0}\right)^{1/2}. \quad (24)$$

Thus ξ^{-1} is the relaxation length of the transverse momentum and φ the rotation angle per unit length of the transverse momentum vector.

The structure of Eq. (20) is the following. The left-hand side contains two terms that come from the relaxation of $\mathbf{m}$ [Eq. (9)] and two terms that come from Joule heating [Eq. (10)]. There are additional quadratic terms that would correspond to the dissipation of the longitudinal and transverse components of the chemical-potential vector $\mathbf{m}$. We verified that these are of second order and can be neglected. The characteristic polynomial of Eq. (20), $P(x) = P_0 + P_1 x + P_2 x^2 + P_3 x^3$, has roots that are close to those of the diffusion equation with only P_1 and P_3, that is, the diffusion equation for $m_\parallel$ without Joule effects,

$$r_1 = -\sqrt{-\frac{P_1}{P_3}} + \frac{P_3 P_0 - P_1}{2P_2\sqrt{-P_1 P_3} + 2P_1 P_3},$$

$$r_2 = \sqrt{-\frac{P_1}{P_3}} - \frac{P_3 P_0 - P_1}{2P_2\sqrt{-P_1 P_3} - 2P_1 P_3},$$

$$r_3 = -\frac{P_0}{P_1}. \quad (25)$$

So, the general solution $\mathcal{F}_0(m_\parallel)$ has the following general form:

$$\mathcal{F}_0(m_\parallel) = a_1 \exp(r_1 x) + a_2 \exp(r_2 x) + a_3 \exp(r_3 x). \quad (26)$$

Referring to Eq. (21), we define $\lambda_{sf} = \sqrt{c_0\tau_{sf}/e}$ and $\lambda_J = \sqrt{c_0/ge}$, which are the characteristic length scales of spin-flip scattering and precession processes. The longitudinal spin-diffusion length $\lambda_{sdl} \approx -r_1^{-1} \approx r_2^{-1}$ is close to λ_{sf}, whereas the relaxation length of transverse momentum ξ^{-1} arises from a combination of both processes. Depending on the ratio λ_J/λ_{sf}, we find two regimes: when λ_J/λ_{sf} is small, $\mathbf{m}_\perp$ decays faster than $m_\parallel$; on the contrary when λ_J is longer than λ_{sf}, then the absorption of $\mathbf{m}_\perp$ is mostly due to spin-flip scattering processes, which relax $m_\parallel$ also, and ξ^{-1} and λ_{sdl} are of similar values (Fig. 2).

To our knowledge, there are no experimental values for λ_J in transport conditions in metallic spin valves. Yet Weber *et al.*[33] measured the precession of the spin polarization of a hot electron beam passing through a ferromagnetic layer of a few nanometers and reported equivalent φ^{-1} of 11 nm for Fe, 50 nm for Ni, and 19 nm for Co. If we follow the theoretical estimates of a few nanometers for λ_J by Zhang *et al.*,[10] λ_J/λ_{sf} may not necessary be small for all material, as λ_{sf} can be of only a few nanometers: for example, in Permalloy λ_{sf} have been measured around 5 nm at room temperature[34] and 3 nm for $Ni_{93}Cr_3$ alloy at 4.2 K.[35] On the other hand, λ_{sf} has been measured to be about 40 nm in cobalt at room temperature[36] so we should be clearly in the regime of strong of $\lambda_J/\lambda_{sf} \ll 1$. We examine further the influence of the ratio λ_J/λ_{sf} on transport measurements by the simulations described in Secs. III and IV.

B. Boundary conditions and solutions

As boundary conditions of the system, we assume continuity of the electrical and chemical potentials, temperature and currents, and the nondivergence of the chemical potential as the length goes to infinity. This means that we do not take into account specular or diffusive scattering due to the interfaces, though they could in theory be inserted into the model through scattering matrix relations (see, e.g., Ref. 5). Generally speaking, as solutions of the equations are a linear combination of exponential terms, these boundary conditions lead to a system of linear equations where the variables are the coefficients of the exponentials, the charge current density j_e and the potential drop ΔV and the temperature drop ΔT between the ends of the system.

We now consider a F/N/F spin valve in a noncollinear configuration (Fig. 2), with the angle θ between the orientations of the layer magnetizations $\mathbf{M}_1$ and $\mathbf{M}_2$. For clarity, we simplify the structure to two equally thin cobalt layers separated by a thin copper layer and connected by copper leads that are much longer than the spin-diffusion length. Calculations are detailed in the Appendix. The continuity conditions at both interfaces lead to 30 [Eqs. (A11)–(A21)]. Replacing the chemical-potential functions by their expressions (A6)–(A10), we obtain a bilinear system from Eqs. (A11)–(A21),

$$\sum_{1 \le i \le 30} \lambda_{ki}\alpha_i = w_k j_e + u_k \Delta T \quad (1 \le k \le 30). \quad (27)$$

The unknown parameters α_i are the potential drop ΔV, the electrical field in the nonmagnetic layers $(\mathcal{E}_{(-)}, \mathcal{E}_N, \mathcal{E}_{(+)})$, and the 24 parameters of the chemical-potential vector in the five layers (see Appendix). For $1 \le k \le 30$, (λ_{ki}), (κ_{kij}), (w_k), and

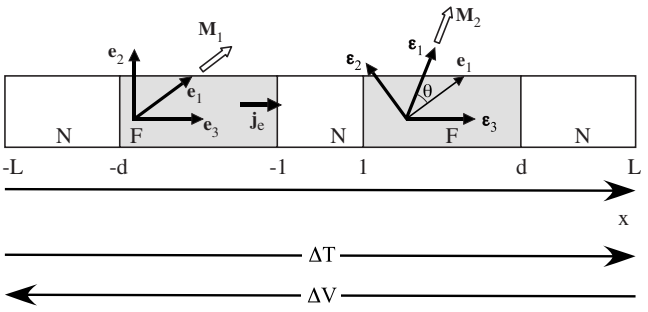

FIG. 3. Schematics of a F/N/F spin valve in noncollinear orientation: $\mathbf{M}_1$ and $\mathbf{M}_2$ are the magnetizations of the two layers, θ is the angle between $\mathbf{M}_1$ and $\mathbf{M}_2$, and $(\mathbf{e}_1,\mathbf{e}_2,\mathbf{e}_3)$ and $(\boldsymbol{\varepsilon}_1,\boldsymbol{\varepsilon}_2,\boldsymbol{\varepsilon}_3)$ are the local orthogonal basis of space, with $\mathbf{e}_3=\boldsymbol{\varepsilon}_3$ normal to both magnetization. ΔT and ΔV are the temperature and potential drops and j_e is the charge current. The ends of the ferromagnetic layers are located at $x=\pm L$, L being long compared to all relaxation lengths, and the interfaces F/N at $x=\pm l$ and $x=\pm d$.

(u_k) are coefficients given by the k_{th} equation.

Now we write the bilinear system in a more comprehensive algebraic expression. We note $\mathbf{S}$ the matrix of (λ_{ki}) coefficients, W the column vector of (w_k) coefficients, and U the column vector of (u_k) coefficients. We decompose the vector of unknown variables X_0, and we write Eq. (27) in the following expression:

$$\mathbf{S}X_0 = Wj_e + U\Delta T. \tag{28}$$

Thus we compute the giant magnetoresistance (GMR) R and the Seebeck coefficient Σ to first order with the formula

$$\Delta V = (\mathbf{S}^{-1}W)(1)j_e + (\mathbf{S}^{-1}U)(1)\Delta T = RI + \Sigma\Delta T. \tag{29}$$

III. RESULTS

A. GMR, thermoelectric power coefficient, and chemical-potential vector

We investigate the response of the structure described in Fig. 3 to ΔT, j_e, and θ. The cross-sectional area of the nanowire is considered to be 100×100 nm^2, the lengths of the nonmagnetic leads are 3000 nm, the ferromagnetic layers are 30 nm thick, and the nonmagnetic spacer layer is 4 nm thick. We use in our calculations the transport parameters of cobalt and copper used by Gravier *et al.*[24] which for convenience are listed in Table I. The dimensionless coefficients β and η define the asymmetry of the spin-dependent conductivity and Seebeck coefficients,

$$\hat{C} = c_0(\hat{I} + \beta\mathbf{M}\cdot\boldsymbol{\sigma}),$$

$$\hat{\varepsilon} = \hat{C}^{-1}\hat{K} = \varepsilon_0(\hat{I} + \eta\mathbf{M}\cdot\boldsymbol{\sigma}).$$

Hence the generalized conductivity is

$$\hat{K} = \hat{C}\hat{\varepsilon} = (c_0\hat{I} + c\mathbf{M}\cdot\boldsymbol{\sigma})(\varepsilon_0\hat{I} + \varepsilon\mathbf{M}\cdot\boldsymbol{\sigma})$$

$$= c_0\varepsilon_0(1+\beta\eta)\hat{I} + c_0\varepsilon_0(\beta+\eta)\mathbf{M}\cdot\boldsymbol{\sigma}.$$

This development yields readily

$$k_0 = (\varepsilon_\uparrow c_\uparrow + \varepsilon_\downarrow c_\downarrow) = \varepsilon_0 c_0(1+\beta\eta),$$

$$k = (\varepsilon_\uparrow c_\uparrow - \varepsilon_\downarrow c_\downarrow) = \varepsilon_0 c_0(\beta+\eta).$$

We use the value of the copper spin-diffusion length found by Doudin *et al.*,[31] owing to the presence of Co impurities in the copper layers produced by electrodeposition. For cobalt, we adjust τ_{sf} to obtain the same scale of $\lambda_{sdl}\approx -r_1^{-1}\approx r_2^{-1}$ of 50 nm. We vary λ_J arbitrarily, even to unrealistic values for cobalt, in order to explore the influence of λ_J/λ_{sf} ratio on the response of the structure, especially on MTGV and double-frequency simulations to be detailed in Secs. III B and III C.

Figures 4 and 5 show the GMR and Seebeck coefficient, respectively, and Figs. 6–8 the dependence of the chemical-potential vector $\mathbf{m}$ on the angle between the two layers for several values of λ_J/λ_{sf}. The GMR peak is affected by the ratio λ_J/λ_{sf}: the larger λ_J/λ_{sf} is, the broader the peak is, and the GMR peak tends toward a cosine shape when $\lambda_J/\lambda_{sf}\geq 0.5$.

As we mentioned previously, when the relaxation of the chemical potential through precession is weak compared to the spin-flip scattering mechanism, then the transverse and longitudinal components decay over the same length, and the situation is analogous to the transmission of light through polarizers. Hence, the cosine dependence appears in this limit. In effect, the transverse component at the $x=-l$ interface, m_2, (Fig. 7) which is in the plane defined by $\mathbf{M}_1$ and $\mathbf{M}_2$, increases with λ_J and tends toward $\sin\theta$. On the contrary, the out-of-plane component of the spin-accumulation vector, m_3 (Fig. 8), vanishes at values of $\lambda_J\geq\lambda_{sf}$. This is because m_3 is essentially created by the spin-current conti-

TABLE I. Numerical values used in the calculations, as used in Gravier *et al.* (Ref. 25) for electrodeposited Co-Cu multilayers.

T (K)	Co	Cu
ρ (Ω m)	$2.64\times10^{-7}+T(2.84\times10^{-9})$	$6.67\times10^{-8}+T(6.86\times10^{-10})$
$\beta=c/c_0$	$0.454-T(1.15\times10^{-4})$	
$\varepsilon_0\varepsilon_N$ (V/K)	$-2.7\times10^{-6}-T(0.1\times10^{-6})$	$-0.084\times10^{-6}T$
$\eta=\varepsilon/\varepsilon_0$	0.41	
l (W/m K)	100	400
λ_{sdl} (nm)	50	40

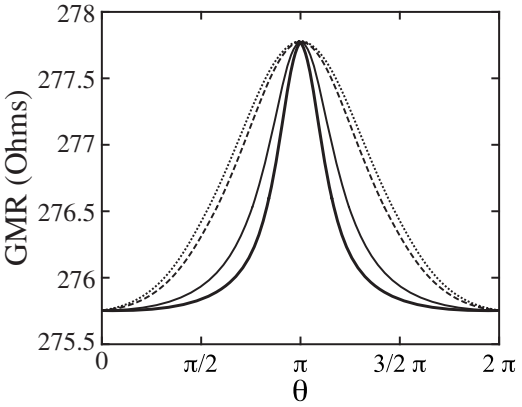

FIG. 4. GMR response of the N/F/N/F/N (3000/30/4/30/3000 nm) spin valve as a function of θ for several values of λ_J/λ_{sf}: 0.02 (solid line with dots), 0.05 (solid line), 0.2 (dashed line), and 0.5 (dotted line).

nuity at interfaces, which links m_3 to m_2 through the parameter φ [Eq. (24)] giving the rotation per unit length. Though m_3 vanishes for large λ_J/λ_{sf}, m_3 reaches a maximum when λ_J/λ_{sf} is close to 0.5. When λ_J is very small compared to λ_{sf}, we are in the regime in which spins that are not eigenstates of the spin Hamiltonian relax quickly. Then, spin accumulation does not develop until the layers are very near the antiparallel configuration, thus resulting in a sharp upturn of the GMR (Fig. 4) and a small accumulation in the transverse component at the interfaces (Fig. 6). Even though we have not taken into account scattering due purely to the interfaces, which would be superposed on the effects described here, our calculation of the GMR response gives comparable results with those given by the treatment using magnetoelectronic circuit theory of Brataas *et al.*[5]

The structure of Eq. (29) suggests a strong similarity in shape between the GMR and the effective Seebeck coefficient, as indeed confirmed by the simulations depicted in Figs. 4 and 5 and by experimental data of GMR and thermoelectric power (TEP) in multilayers.[37] The order of magnitude of the TEP is about 25 μV/K at 300 K, whereas the resistance is about 276 Ω. This means that a temperature

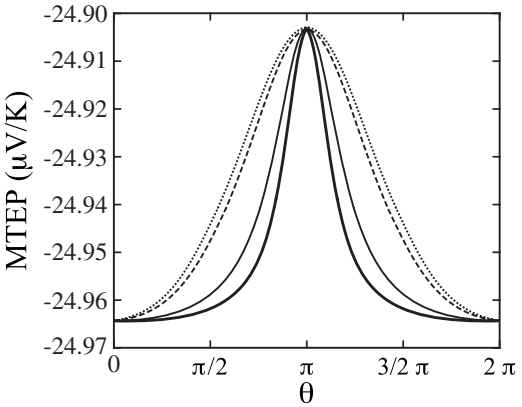

FIG. 5. Seebeck coefficient of the N/F/N/F/N (3000/30/4/30/3000 nm) spin valve as a function of θ for several values of λ_J/λ_{sf}: 0.02 (solid line with dots), 0.05 (solid line), 0.2 (dashed line), and 0.5 (dotted line).

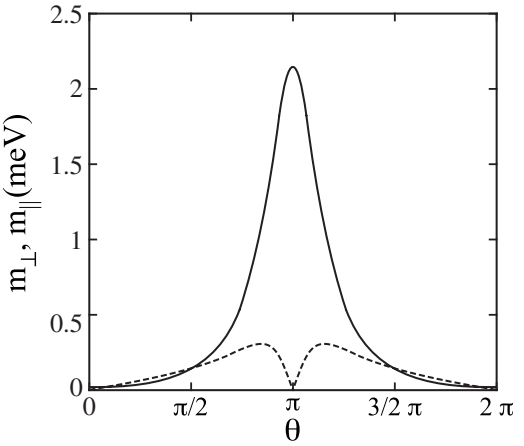

FIG. 6. Modulus of $m_\perp$ (dashed line) and $m_\parallel$ (solid line) at F/N interface for a current of 6×10^6 A/cm^2, ΔT of 1 K, and $\lambda_J/\lambda_{sf}=0.05$.

drop of 1 K creates the same voltage drop as a current of 20 nA in the nanopillar of 100×100 nm^2, that is, a current density of 2×10^2 A/cm^2 only. The spin-accumulation vector created by the temperature gradient presents the same angular dependence as that created by charge current, but its amplitude is about 10^{-9} eV for a temperature drop of 1 K, compared to 10^{-4} eV for a current of 100 μA. Hence it is practically impossible to create spin torque with a temperature gradient in metallic spin valves.

B. MTGV simulation

Gravier *et al.*[24] showed that MTGV is highly sensitive to the temperature-dependent change in the spin-mixing rates between the up and down channels. In Ref. 24, spin mixing is introduced in a representation where spin is only in up and down states. Collisions with magnons induce spin flips between these two states. Here we are considering the precession of spins around the exchange field, which corresponds to transitions between the up and down states of the spin quantized along the axis parallel to the exchange field, the rate of which are given by the Rabi formula. Thus we expect

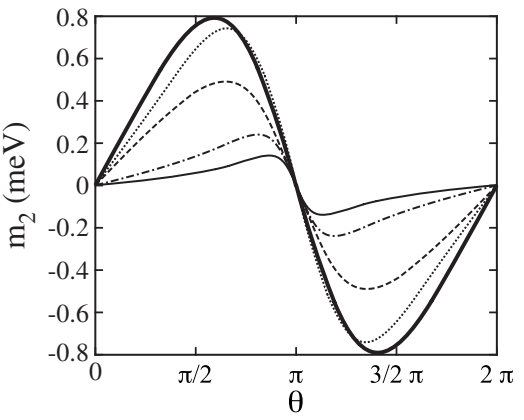

FIG. 7. Transverse component m_2, parallel to $\mathbf{M}_1\times(\mathbf{M}_1\times\mathbf{M}_2)$, as a function of θ, for several λ_J/λ_{sf}: 0.02 (solid line), 0.05 (dashed-dotted line), 0.2 (dashed line), 0.5 (dotted line), and 1 (gray dots).

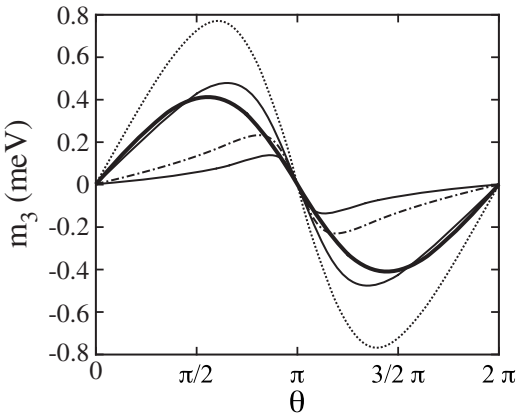

FIG. 8. Out-of-plane transverse component m_3, parallel to $\mathbf{M}_1 \times \mathbf{M}_2$, as a function of θ, for several λ_J/λ_{sf}: 0.02 (solid line), 0.05 (dashed-dotted line), 0.2 (dashed line), 0.5 (dotted line), and 1 (circles).

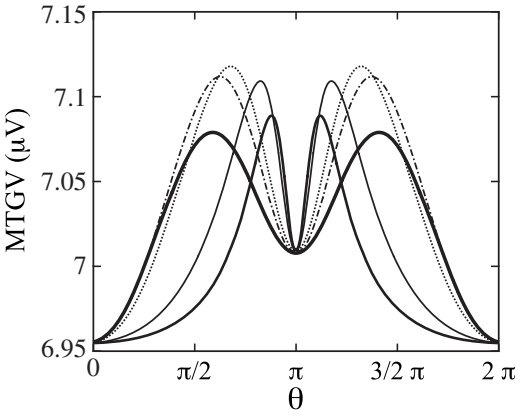

FIG. 9. MTGV response as a function of θ for several λ_J/λ_{sf}: 0.02 (solid line with dots), 0.05 (solid line), 0.2 (dots), 0.5 (dashed-dotted line), and 1 (circles).

that the MTGV is sensitive to the transverse component $\mathbf{m}_\perp$ and to its relaxation.

In order to reproduce the experimental protocol in simulation we add to the base temperature T_0 (300 K) and to the temperature gradient ΔT a small sinusoidal temperature oscillation with an amplitude of 1 K. Thus, every coefficient of transport, provided it has temperature dependence, is oscillating with T_0 at the chopping frequency. We set the current density at 4×10^6 A/cm^2, which corresponds to a dc of 400 μA through the nanopillar and is the order of magnitude of the current used in MTGV experiments.[20] In this calculation, the MTGV is given by the first harmonic of the voltage response ΔV [Eq. (29)].

The dependence of MTGV on the angle θ is displayed in Fig. 9. The MTGV curves correspond to several values of λ_J. We identify the contribution of the transverse component of $\mathbf{m}$ to the MTGV as follows. When we compare the calculated MTGV with the transverse components of $\mathbf{m}_\perp$ (Figs. 7 and 8), we notice that the MTGV peaks behave like m_3 (Fig. 8). We recall that m_3 is induced purely by precession of $\mathbf{m}_\perp$. Like m_3, the MTGV peak is the largest when λ_J is about half of λ_{sf}. Both decrease at larger values of λ_J because the spin-relaxation wave vector φ [Eq. (23)] decreases with increasing λ_J. Also, MTGV peaks broaden toward $\theta=\pm\pi/2$ when λ_J increases, as the maxima of $m_\perp$ do (Fig. 9).

When we compare these simulations to the experimental data obtained in five-bilayer structures of alternating Co/Cu layers embedded in a copper nanopillar,[38] we find that the observed MTGV peaks are often of about the same order of magnitude but sometimes an order of magnitude larger than the simulation. The discrepancy may arise from the fact that the layers and interfaces are inhomogeneous in structures obtained by electrodeposition and, as we will discuss below, the inhomogeneities in the magnetization is expected to enhance the MTGV signal. It was pointed out that the observed peaks in the MTGV measurement occur when layers switch reversibly from parallel to antiparallel configurations and vice versa (that is from $\theta=0$ to $\theta=\pi$), i.e., when noncollinear states may be reached in a quasistatic field sweep.

We have studied the dependence of MTGV on the constitutive parameters of transport, especially those that change with temperature. It appears from the simulations that the MTGV is essentially caused by the temperature dependence of λ_J. As $\lambda_J=\sqrt{c_0/ge}$, it depends on temperature at room temperature essentially because of the conductivity dependence,

$$\frac{\partial\lambda_J}{\partial T}\lambda_J = \frac{1}{2c_0}\frac{\partial c_0}{\partial T} - \frac{1}{2g}\frac{\partial g}{\partial T}.$$

The relation between MTGV and transverse moment becomes clear when we make the derivative of Eq. (29) with respect to λ_J,

$$\frac{\partial\Delta V}{\partial\lambda_J} = -\mathbf{S}^{-1}\frac{\partial\mathbf{S}}{\partial\lambda_J}\Delta V_0. \tag{30}$$

ΔV_0 is the voltage response at the average of the oscillating temperature T_0 in Eq. (29). The matrix $\frac{d\mathbf{S}}{d\lambda_J}$ contains only terms coming from the derivative of ξ and φ. This implies that the MTGV signal is proportional to the transverse moment [see Eqs. (A13) and (A14)]. In order to make more explicit the importance of the relaxation of the transverse moment on the MTGV signal, we show in Fig. 10 what the

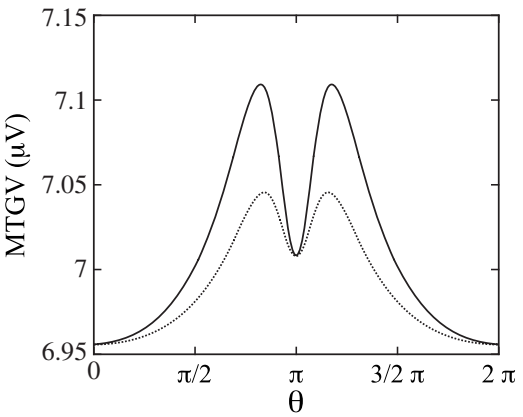

FIG. 10. MTGV signal dependence on the derivative $d\lambda_J/dT$. (a) (solid line) $\lambda_J^{-1}(d\lambda_J/dT)=0.75\times10^{-3}$ K^{-1} and (b) (dotted line) $d\lambda_J/dT=0$. Here $\lambda_J/\lambda_{sf}=0.05$.

MTGV response becomes when the temperature dependence of λ_J is canceled. There is still a signal, with similar angular dependence. It arises simply from the temperature dependence of the conductivity.

C. Nonlinearity and second-harmonic signal

Oscillations of the layers' magnetizations due to oscillating current can introduce a signal at double frequency of the oscillating current. Indeed, spin torque and the induced field created by the current produce a perturbation of the equilibrium position imposed by the external field on the layers. Following Barnas *et al.*,[39] we determine the momentum transferred to the free layer (the calculations are carried out assuming one layer is fixed) as the difference between the spin-current entering and leaving the layer,

$$\Delta \boldsymbol{\tau} = \frac{\mu_B}{e}[\mathbf{j_m}(L) - \mathbf{j_m}(l)]S, \tag{31}$$

where S is the cross-sectional area of the nanopillar and μ_B is the Bohr magneton. Thus when we compute the equivalent field that would be applied to the magnetization in the presence of such an oscillating current, we find it to be about 100 G. So the induced field due to current passing through the circuit coil is small compared to spin torque (0.1 G compared to 100 G), thus we consider only the deviation of theta created by the spin torque.

Now we refer to the formula of Kovalev *et al.*[26] and estimate $\delta\theta$ with

$$|\delta\theta| = \left| \frac{c_0\mu_B}{2e^2 L\gamma M_s^2(N_2N_3 - N_{23}^2)}\left(N_{23}\frac{dm_2}{dx} + N_3\frac{dm_3}{dx}\right)\sin(\theta)\right|, \tag{32}$$

where γ is the gyromagnetic ratio, L is the length of the layer, M_s is the saturation magnetization, and N_i are the demagnetization coefficients of the free energy at equilibrium of the macrospin magnetization with which we model the free layer,

$$F(\mathbf{M}) = F(M_1) + \frac{N_2}{2}M_2^2 + \frac{N_3}{2}M_3^2 + N_{23}M_2M_3. \tag{33}$$

In Eq. (32), we have neglected all terms at the frequency of the current for this is far below the resonance frequency. For the calculation we chose $M_s = 10^6$ A m^{-1}, we set d at 30 nm, and we chose $N_2 = 0.2\mu_0$, $N_3 = \mu_0$, and $N_{23} = 0$ (N_i/μ_0 are between 0 and 1). The perturbation of the angle θ is depicted in Fig. 11 for several values of λ_J/λ_{sf}. $\delta\theta$ is about 10^{-2} rad in magnitude. Like the spin torque, it decreases with increasing λ_J, that is, with decreasing strength of the interaction between conduction electrons and the local magnetization. Figure 12 shows the dependence on θ of the modulus of the second-harmonic Fourier coefficient of the ΔV response for several values of λ_J. The double-frequency response is extremely sensitive to $\delta\theta$: it gives about a few microvolts for a deviation of only 10^{-2} rad. Compared to this response, the perturbation voltage due to the quadratic terms, neglected in Eq. (20), was found to be of about 10^{-8} V for a current density of 6×10^6 A/cm^2. The peaks of MTGV are located between the maxima of $\delta\theta$ and of $\frac{\partial R}{\partial\theta}$. The peaks of the second harmonic behave the same way as those of the MTGV and occur at the same angles (Fig. 9): they get broader and move toward $\theta = \pm\pi/2$ as λ_J/λ_{sf} increases. Yet whereas the amplitude of the MTGV is at a maximum when λ_J/λ_{sf} is close to 0.5, the second harmonic decreases much more quickly with λ_J. This is due to the fact that the second harmonic detects the spin current and not the chemical potential. When we compare Fig. 12 with Fig. 4, we find that the second-harmonic peaks occur when GMR is about halfway through the rise. The position of the peaks on a θ scale tends toward π when λ_J/λ_{sf} decreases and the peaks get sharper and bigger. We notice also that the ratio between the width and the height of the peaks is a very sensitive function of λ_J/λ_{sf}. So, if we are able to control the angle θ between the two layer magnetizations, the double-frequency measurement would enable us to determine λ_J: either by looking at the position of the maximum of the peak, which give a rather rough estimation, or by computing the ratio between the width and the height of the peak, which should be a more

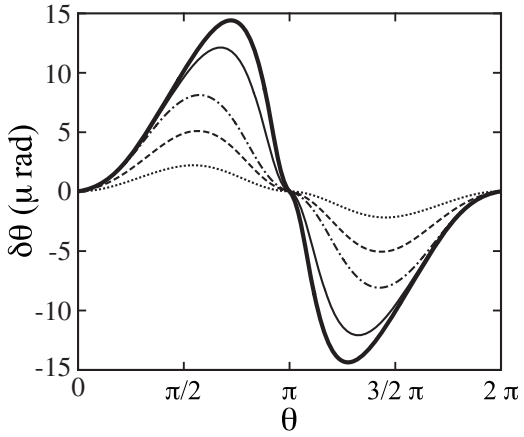

FIG. 11. $\delta\theta$ as a function of the equilibrium angle between the layers, $j_e = 6\times10^6$ A/cm^2, $\Delta T = 0$ K, and λ_J/λ_{sf}: 0.02 (solid line with dots), 0.05 (solid line), 0.2 (dashed-dotted line), 0.5 (dashed line), and 2 (gray dots).

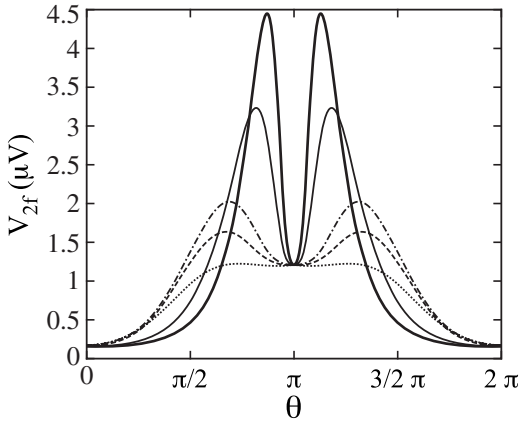

FIG. 12. Calculation of double-frequency response as a function of θ and λ_J, $j_e = 6\times10^6$ A/cm^2, $\Delta T = 0$ K, and λ_J/λ_{sf}: 0.02 (solid line with dots), 0.05(solid line), 0.2 (dashed-dotted line), 0.5 (dashed line), and 2 (gray dots).

precise method, especially for small λ_J/λ_{sf}. While this analysis enables us to point to a possible measurement method, the interpretation of actual data will have to be done keeping in mind that the present predictions result from a simple diffusive model and that a better account of interface scattering might be necessary for the data to yield a correct value of λ_J.[8,26]

IV. DISCUSSION

As we mention before, the macrospin approximation used to solve the constitutive equation lets us understand the physics underlined by equations but it is a rough approximation. In fact, spatial inhomogeneities in the local layer magnetization orientation induce relaxation of the chemical potential through precession all through the layer and not only at the F/N interface. In other words, the spin-mixing process is enhanced by magnetization inhomogeneity.

The special variation in magnetization introduces new terms in Eq. (18) that becomes

$$2\left[c_0\frac{d\mathcal{E}}{dx}-k_0\frac{d^2T}{dx^2}+c\mathbf{M}\cdot\frac{1}{e}\frac{d^2\mathbf{m}}{dx^2}+c\frac{d\mathbf{M}}{dx}\cdot\frac{1}{e}\frac{d\mathbf{m}}{dx}\right]=0, \tag{34}$$

$$2\left[\left(c\frac{d\mathcal{E}}{dx}-k\frac{d^2T}{dx^2}\right)\cdot\mathbf{M}+\left(c\mathcal{E}-k\frac{dT}{dx}\right)\cdot\frac{d\mathbf{M}}{dx}+c_0\frac{1}{e}\frac{d^2\mathbf{m}}{dx^2}\right]=\frac{\mathbf{m}}{\tau_{sf}}+g\mathbf{M}\wedge\mathbf{m}, \tag{35}$$

$$2\left[T_0k_0\frac{d\mathcal{E}}{dx}-l_0\frac{d^2T}{dx^2}+T_0k\mathbf{M}\cdot\frac{1}{e}\frac{d^2\mathbf{m}}{dx^2}+T_0k\frac{d\mathbf{M}}{dx}\cdot\frac{1}{e}\frac{d\mathbf{m}}{dx}\right]=\left(E(x)\cdot\hat{I}+\frac{1}{e}\frac{d\hat{\mu}}{dx}\right):\hat{j}. \tag{36}$$

In order to keep the expressions not too heavy, we overlook Joule heating terms ($P_0=P_2=0$). This leads us to modify the differential equations [Eqs. (20) and (21)] so as to obtain

$$\frac{1}{e}\left(\frac{u}{k_0}\frac{T_0kk_0-l_0c}{T_0k_0^2-l_0c_0}-\frac{kc}{k_0}\right)\left(\frac{d^2m_\parallel}{dx^2}+\frac{d\mathbf{m}_\perp}{dx}\frac{d\mathbf{M}}{dx}\right)+\frac{c_0}{e}\frac{d^2m_\parallel}{dx^2}=\frac{m_\parallel}{2\tau_{sf}} \tag{37}$$

$$\left(\frac{u}{k_0}\frac{T_0kk_0-l_0c}{T_0k_0^2-l_0c_0}-\frac{kc}{k_0}\right)\frac{dm_\parallel}{edx}\frac{d\mathbf{M}}{dx}+\frac{1}{2}\left(\frac{k}{k_0}j_e+\frac{j_qk_0-l_0j_e}{T_0k_0^2-l_0c_0}\right)\frac{d\mathbf{M}}{dx}+\frac{c_0}{e}\frac{d^2\mathbf{m}_\perp}{dx^2}=\frac{\mathbf{m}_\perp}{2\tau_{sf}}+\frac{g}{2}\mathbf{M}\wedge\mathbf{m}. \tag{38}$$

Without solving these equations, we can already discuss their significance. The transverse and longitudinal components of $\mathbf{m}$ are now coupled by terms depending on the gradient of $\mathbf{M}$. Qualitatively, when $\frac{d\mathbf{M}}{dx}$ is small, i.e., when the typical length scale of variation in $\mathbf{M}$ is long compared to λ_{sf}, the longitudinal component relaxes before there is much change in the magnetization orientation. So the two equations are decoupled and the relaxation lengths λ_{sdl} and ξ^{-1} are not very much affected. On the contrary, when the typical length scale of variation in $\mathbf{M}$ is of the same order or even shorter than λ_{sf}, a great part of $m_\parallel$ is transferred to $\mathbf{m}_\perp$ due to the reorientation of $\mathbf{M}$ and relaxation is dominated by spin precession. This is expressed in Eqs. (37) and (38) by the fact that coupling terms become important. When we calculate the roots of the characteristic polynomial of Eq. (35), we find that ξ^{-1} increases and λ_{sdl} decreases. Thus, relaxation through spin mixing is dramatically enhanced with an inhomogeneous $\mathbf{M}$.

V. CONCLUSION

We proposed a diffusive model to describe thermoelectrical transport in magnetic multilayers using the linear space defined by Pauli matrices to describe the spin current and the generalized electrochemical potential. We applied this model to a spin valve, assuming one layer pinned, in order to investigate the origin of the sharp field-dependent peaks in the experimentally observed MTGV, a measurement of the temperature derivative of the resistance. These simulations confirm that MTGV is able to detect spin-mixing effects through the temperature dependence of the length scale λ_J that defines the relaxation of the spin accumulation normal to the magnetization. At room temperature, a dominant contribution to this temperature dependence is that of the conductivity. We compute also the second-harmonic amplitude of the voltage response created by the ac spin-torque perturbation on the magnetization of the layers. Our estimate leads to several microvolts of response for a current density of several 10^6 A/cm^2, that is, detectable at current densities below the critical values that are able to destabilize the magnetization of the layers and far away from resonance also. Specifically, this second-harmonic response has a strong dependence on λ_J/λ_{sf}; thus, it may provide a new measure of the relaxation length λ_J. Finally, we discuss the possibility of a large enhancement of these spin-mixing effects by magnetic inhomogeneities. Thus MTGV and the second-harmonic response are measurements that are able to characterize the relaxation of the transverse spin accumulation.

APPENDIX

The studied structure (Fig. 3) consists in a spin-valve F/N/F. We note θ the angle between the orientations of the layer magnetizations. $(\mathbf{e}_1,\mathbf{e}_2,\mathbf{e}_3)$ and $(\boldsymbol{\varepsilon}_1,\boldsymbol{\varepsilon}_2,\boldsymbol{\varepsilon}_3)$ are the local bases for left and right cobalt magnetizations, with $\mathbf{e}_1$ and $\boldsymbol{\varepsilon}_1$ parallel to local magnetization. The relations between the bases are

$$\boldsymbol{\varepsilon}_1=\cos(\theta)\mathbf{e}_1+\sin(\theta)\mathbf{e}_2,$$

$$\boldsymbol{\varepsilon}_2=-\sin(\theta)\mathbf{e}_1+\cos(\theta)\mathbf{e}_2,$$

$$\boldsymbol{\varepsilon}_3 = \mathbf{e}_3. \tag{A1}$$

1. Expression of E, dT/dx, and currents in a ferromagnetic layer

We refer to the notations introduced in Fig. 1. In one ferromagnetic layer, the expressions of the generalized electrical field, the gradient of temperature, and the currents are given by integrating Eq. (9) and replacing the various expressions of Eq. (18),

$$\mathcal{E} = \frac{k_0}{2\tau u}\mathcal{F}(m_\parallel) - \frac{v}{eu}\frac{dm_\parallel}{dx}, \tag{A2}$$

$$\frac{dT}{dx} = \frac{c_0}{2u\tau_{\mathrm{sf}}}\mathcal{F}(m_\parallel) + \frac{cu - c_0 v}{ek_0 u}\frac{dm_\parallel}{dx} - \frac{j_e}{2k_0}, \tag{A3}$$

$$\frac{j_q}{2} = P_1\mathcal{F}(m_\parallel) + P_3\frac{dm_\parallel}{dx} + \frac{l_0}{2k_0}j_e, \tag{A4}$$

$$\frac{\mathbf{j_m}}{2} = \left(\frac{F(m_\parallel)}{2\tau_{\mathrm{sf}}} + \frac{k}{2k_0}j_e\right)\mathbf{e}_1 + \frac{c_0}{e}\frac{d\mathbf{m}_\perp}{dx}. \tag{A5}$$

2. Expression of solutions

From the forms of solution found in Eqs. (17), (23), and (26) we express the chemical potential in each layer. In the right ferromagnetic layer, the chemical potential $\mathbf{n} = (n_1, n_2, n_3)$ is decomposed on the base $(\boldsymbol{\varepsilon}_1, \boldsymbol{\varepsilon}_2, \boldsymbol{\varepsilon}_3)$. (n_2, n_3) can be written in the form below, where $\mathbf{n}_{(+)}$ and $\mathbf{n}_{(-)}$ are complex numbers,

$$\begin{aligned} n_2 &= \mathrm{Re}(\mathbf{n}_{(+)}e^{(\xi+i\varphi)(x-l)} + \mathbf{n}_{(-)}e^{-(\xi+i\varphi)(x-l)}), \\ n_3 &= \mathrm{Im}(\mathbf{n}_{(+)}e^{(\xi+i\varphi)(x-l)} + \mathbf{n}_{(-)}e^{-(\xi+i\varphi)(x-l)}), \end{aligned} \tag{A6}$$

$$\mathcal{F}(n_1) = a_1 e^{r_1(x-l)} + a_2 e^{r_2(x-l)} + a_3 e^{r_3(x-l)}. \tag{A7}$$

In the left ferromagnetic layer, the chemical potential $\mathbf{m} = (m_1, m_2, m_3)$ is decomposed on the base $(\mathbf{e}_1, \mathbf{e}_2, \mathbf{e}_3)$. (m_2, m_3) can be written in the form of Eq. (A8), where $\mathbf{m}_{(+)}$ and $\mathbf{m}_{(-)}$ are complex numbers,

$$\begin{aligned} m_2 &= \mathrm{Re}(\mathbf{m}_{(+)}e^{(\xi+i\varphi)(x-l)} + \mathbf{m}_{(-)}e^{-(\xi+i\varphi)(x-l)}), \\ m_3 &= \mathrm{Im}(\mathbf{m}_{(+)}e^{(\xi+i\varphi)(x-l)} + \mathbf{m}_{(-)}e^{-(\xi+i\varphi)(x-l)}), \end{aligned} \tag{A8}$$

$$\mathcal{F}(m_1) = b_1 e^{r_1(x-l)} + b_2 e^{r_2(x-l)} + b_3 e^{r_3(x-l)}. \tag{A9}$$

In the nonmagnetic spacer, in the base $(\mathbf{e}_1, \mathbf{e}_2, \mathbf{e}_3)$, the chemical-potential vector $\mathbf{p}$ is linked to two vectors $\mathbf{A} = (A_1, A_2, A_3)$ and $\mathbf{B} = (B_1, B_2, B_3)$,

$$\mathbf{p} = \mathbf{A}\cosh(qx) + \mathbf{B}\sinh(qx). \tag{A10}$$

In the nonmagnetic electrodes, the chemical potential taken decreases exponentially from the F/N interfaces to the extremities of the electrodes. In the left electrode it is equal to $\mathbf{p}^{(-)}\exp[q(x-d)]$, with $\mathbf{p}^{(-)} = (p_1^{(-)}, p_2^{(-)}, p_3^{(-)})$ in $(\mathbf{e}_1, \mathbf{e}_2, \mathbf{e}_3)$. In the right electrode it is equal to $\mathbf{p}^{(+)}\exp[-q(x-d)]$, with $\mathbf{p}^{(+)} = (p_1^{(+)}, p_2^{(+)}, p_3^{(+)})$ in $(\boldsymbol{\varepsilon}_1, \boldsymbol{\varepsilon}_2, \boldsymbol{\varepsilon}_3)$. We will also note $\mathcal{E}_N$ and $\mathcal{E}_{(+)}\mathcal{E}_{(-)}$ the electrical field in the nonmagnetic spacer and the right electrode and the left electrode.

3. Boundary condition matrix

Using expressions (A2)–(A5), we express the continuity of potential and currents on both interfaces at ± 1: chemical potential,

$$\begin{aligned} m_1(-l) &= A_1\cosh(ql) - B_1\sinh(ql), \\ m_2(-l) &= A_2\cosh(ql) - B_2\sinh(ql), \\ m_3(-l) &= A_3\cosh(ql) - B_3\sinh(ql), \\ n_1(l)\cos(\theta) - n_2(l)\sin(\theta) &= A_1\cosh(ql) + B_1\sinh(ql), \\ n_1(l)\sin(\theta) + n_2(l)\cos(\theta) &= A_2\cosh(ql) + B_2\sinh(ql), \\ n_3(l) &= A_3\cosh(ql) + B_3\sinh(ql), \end{aligned} \tag{A11}$$

spin current,

$$\begin{aligned} \frac{\mathcal{F}(m_1)(-l)}{2\tau_{\mathrm{sf}}} + \frac{k}{2k_0}j_e &= \frac{c_N q}{e}[-A_1\sinh(ql) + B_1\cosh(ql)], \\ \frac{c_0}{e}\frac{dm_2}{dx}(-l) &= \frac{c_N q}{e}[-A_2\sinh(ql) + B_2\cosh(ql)], \\ \frac{c_0}{e}\frac{dm_3}{dx}(-l) &= \frac{c_N q}{e}[-A_3\sinh(ql) + B_3\cosh(ql)], \end{aligned} \tag{A13}$$

$$\begin{aligned} \frac{\mathcal{F}(n_1)(l)}{2\tau_{\mathrm{sf}}} + \frac{k}{2k_0}j_e &= \frac{c_N q}{e}\{[A_1\sinh(ql) + B_1\cosh(ql)]\cos(\theta) \\ &\quad + [A_2\sinh(ql) + B_2\cosh(ql)]\sin(\theta)\}, \\ \frac{c_0}{e}\frac{dn_2}{dx}(l) &= \frac{c_N q}{e}\{-[A_1\sinh(ql) + B_1\cosh(ql)]\sin(\theta) \\ &\quad + [A_2\sinh(ql) + B_2\cosh(ql)]\cos(\theta)\}, \\ \frac{c_0}{e}\frac{dn_3}{dx}(l) &= \frac{c_N q}{e}[A_3\sinh(ql) + B_3\cosh(ql)], \end{aligned} \tag{A14}$$

and heat current,

$$\begin{aligned} P_1\mathcal{F}(m_1)(-l) + P_3\frac{dm_1}{dx}(-l) + \frac{l_0}{2k_0}j_e \\ = \left(T_0 k_N - \frac{l_N c_N}{k_N}\right)\mathcal{E}_N + \frac{l_N}{2k_N}j_e, \end{aligned}$$

$$P_1\mathcal{F}(n_1)(l) + P_3\frac{dn_1}{dx}(l) + \frac{l_0}{2k_0}j_e = \left(T_0k_N - \frac{l_Nc_N}{k_N}\right)\mathcal{E}_N + \frac{l_N}{2k_N}j_e. \tag{A15}$$

We obtain equations of the same form when expressing the continuity of potential and currents on the interfaces between ferromagnetic layers and nonmagnetic electrodes at $\pm d$: chemical potential,

$$\begin{aligned} m_1(-d) &= p_1^{(-)}, \\ m_2(-d) &= p_2^{(-)}, \\ m_3(-d) &= p_3^{(-)}, \end{aligned} \tag{A16}$$

$$\begin{aligned} n_1(d) &= p_1^{(+)}, \\ n_2(d) &= p_2^{(+)}, \\ n_3(d) &= p_3^{(+)}, \end{aligned} \tag{A17}$$

$$\begin{aligned} \frac{\mathcal{F}(m_1)(-d)}{2\tau_{\mathrm{sf}}} + \frac{k}{2k_0}j_e &= \frac{c_Nq}{e}p_1^{(-)}, \\ \frac{c_0}{e}\frac{dm_2}{dx}(-d) &= \frac{c_Nq}{e}p_2^{(-)}, \\ \frac{c_0}{e}\frac{dm_3}{dx}(-d) &= \frac{c_Nq}{e}p_3^{(-)}, \end{aligned} \tag{A18}$$

spin current,

$$\begin{aligned} \frac{\mathcal{F}(n_1)}{2\tau_{\mathrm{sf}}}(d) + \frac{k}{2k_0}j_e &= -\frac{c_Nq}{e}p_1^{(+)}, \\ \frac{c_0}{e}\frac{dn_2}{dx}(d) &= -\frac{c_Nq}{e}p_2^{(+)}, \\ \frac{c_0}{e}\frac{dn_3}{dx}(d) &= -\frac{c_Nq}{e}p_3^{(+)}, \end{aligned} \tag{A19}$$

and heat current,

$$\begin{aligned} P_1\mathcal{F}(m_1)(-d) + P_3\frac{dm_1}{dx}(-d) + \frac{l_0}{2k_0}j_e &= \left(T_0k_N - \frac{l_Nc_N}{k_N}\right)\mathcal{E}_{(-)} + \frac{l_N}{2k_N}j_e, \\ P_1\mathcal{F}(n_1)(d) + P_3\frac{dn_1}{dx}(d) + \frac{l_0}{2k_0}j_e &= \left(T_0k_N - \frac{l_Nc_N}{k_N}\right)\mathcal{E}_{(+)} + \frac{l_N}{2k_N}j_e. \end{aligned}$$

Finally we write the continuity of temperature and electrostatic potential over the structure: temperature,

$$\begin{aligned} \Delta T = &\int_{-d}^{-l}\left(\frac{c_0}{2u\tau_{sf}}\mathcal{F}(m_1) + \frac{cu - c_0v}{ek_0u}\frac{dm_1}{dx}\right)dx \\ &+ \int_{l}^{d}\left(\frac{c_0}{2u\tau_{\mathrm{sf}}}\mathcal{F}(n_1) + \frac{cu - c_0v}{ek_0u}\frac{dn_1}{dx}\right)dx - \frac{(d-l)}{k_0}j_e \\ &+ 2l\frac{c_N}{k_N}\mathcal{E}_N - l\frac{j_e}{k_N} + (L-d)\frac{c_N}{k_N}(\mathcal{E}_{(+)} + \mathcal{E}_{(-)}) - (L-d)\frac{j_e}{k_N}, \end{aligned} \tag{A20}$$

and electrostatic potential,

$$\begin{aligned} -\Delta V = &\int_{-d}^{-l}\left(\frac{k_0}{2u\tau_{\mathrm{sf}}}\mathcal{F}(m_1) - \frac{v}{eu}\frac{dm_1}{dx}\right)dx + \int_{l}^{d}\left(\frac{k_0}{2u\tau_{\mathrm{sf}}}\mathcal{F}(n_1)\right. \\ &\left. - \frac{v}{eu}\frac{dn_1}{dx}\right)dx + 2l\mathcal{E}_N + (L-d)(\mathcal{E}_{(+)} + \mathcal{E}_{(-)}). \end{aligned} \tag{A21}$$

[1] L. Berger, Phys. Rev. B **54**, 9353 (1996).
[2] J. J. Slonczewski, J. Magn. Magn. Mater. **159**, L1 (1996).
[3] M. D. Stiles and J. Miltat, in *Spin Dynamics in Confined Magnetic Structures III*, Topics in Applied Physics Vol. 101, edited by B. Hillebrands and A. Thiaville (Springer-Verlag, Berlin, 2006), pp. 225–308.
[4] T. Valet and A. Fert, Phys. Rev. B **48**, 7099 (1993).
[5] A. Brataas, F. E. W. Bauer, and P. J. Kelly, Phys. Rep. **427**, 157 (2006).
[6] J. C. Slonczewski, J. Magn. Magn. Mater. **247**, 324 (2002).
[7] A. Shpiro, P. Levy, and S. Zhang, Phys. Rev. B **67**, 104430 (2003).
[8] J. Zhang, P. M. Levy, S. Zhang, and V. Antropov, Phys. Rev. Lett. **93**, 256602 (2004).
[9] M. D. Stiles and A. Zangwill, Phys. Rev. B **66**, 014407 (2002).
[10] S. Zhang, P. M. Levy, and A. Fert, Phys. Rev. Lett. **88**, 236601 (2002).
[11] M. Johnson and R. H. Silsbee, Phys. Rev. Lett. **55**, 1790 (1985).
[12] M. Johnson and R. H. Silsbee, Phys. Rev. B **35**, 4959 (1987).
[13] M. Johnson and J. Byers, Phys. Rev. B **67**, 125112 (2003).
[14] J.-E. Wegrowe, M. C. Ciornei, and H.-J. Drouhin, J. Phys.: Condens. Matter **19**, 165213 (2007).
[15] See, e.g., S. J. Blundell and K. M. Blundell, *Concepts in Thermal Physics* (Oxford University Press, New York, 2006), Chap. 34.
[16] J.-Ph. Ansermet, IEEE Trans. Magn. **44**, 329 (2008).
[17] A. Fert and I. A. Campbell, Phys. Rev. Lett. **21**, 1190 (1968).
[18] T. Farrell and D. Greig, J. Phys. C **1**, 1359 (1968).
[19] J.-Ph. Ansermet, J. Phys.: Condens. Matter **10**, 6027 (1998).
[20] Moosa Hatami, Gerrit E. W. Bauer, Qinfang Zhang, and Paul J. Kelly, Phys. Rev. Lett. **99**, 066603 (2007).
[21] J. Zhang and P. M. Levy, Phys. Rev. B **71**, 184417 (2005).
[22] P. M. Levy and J. Zhang, Phys. Rev. B **70**, 132406 (2004); **73**, 069901(E) (2006).
[23] P. M. Levy and J. Zhang, J. Phys.: Condens. Matter **16**, S5601 (2004).

[24] L. Gravier, S. Serrano-Guisan, and J.-Ph. Ansermet, J. Appl. Phys. **97**, 10C501 (2005).
[25] L. Gravier, S. Serrano-Guisan, F. Reuse, and J.-Ph. Ansermet, Phys. Rev. B **73**, 024419 (2006).
[26] A. Kovalev, G. E. W. Bauer, and A. Brataas, Phys. Rev. B **75**, 014430 (2007).
[27] N. W. Ascroft and N. D. Mermin, *Solid State Physics* (Saunders, Philadelphia, 1976), Chap. 13.6.
[28] Z. C. Wang, G. Su, and S. Gao, Phys. Rev. B **63**, 224419 (2001).
[29] F. J. Jedema, A. T. Filip, and B. J. van Wees, Nature (London) **410**, 345 (2001).
[30] J. Bass and W. Pratts, J. Phys.: Condens. Matter **19**, 183201 (2007).
[31] B. Doudin, A. Blondel, and J.-Ph. Ansermet, J. Appl. Phys. **79**, 6090 (1996).
[32] L. Piraux, S. Dubois, C. Marchal, J. M. Beuken, L. Filipozzi, J. F. Despres, K. Ounadjela, and A. Fert, J. Magn. Magn. Mater. **156**, 317 (1996).
[33] W. Weber, S. Riesen, and H. C. Siegmann, Science **291**, 1015 (2001).
[34] W. P. Pratt, S. D. Steenwyk, S. Y. Hsu, W. C. Chiang, A. C. Schaefer, R. Loloee, and J. Bass, IEEE Trans. Magn. **33**, 3505 (1997).
[35] W. Park, R. Loloee, J. A. Caballero, W. P. Pratt, P. A. Schroeder, J. Bass, A. Fert, and C. Vouille, J. Appl. Phys. **85**, 4542 (1999).
[36] L. Piraux, S. Dubois, A. Fert, and L. Belliard, Eur. Phys. J. B **4**, 413 (1998).
[37] L. Gravier, S. Serrano-Guisan, F. Reuse, and J.-Ph. Ansermet, Phys. Rev. B **73**, 052410 (2006).
[38] S. Serrano-Guisan, L. Gravier, and J.-Ph. Ansermet, Mater. Sci. Eng., B **126**, 292 (2006).
[39] J. Barnaś, A. Fert, M. Gmitra, I. Weymann, and V. K. Dugaev, Phys. Rev. B **72**, 024426 (2005).